Noise-Aware Training for Analog-Inspired Output-Layer Encodings Under Inference Noise

Analog NN Benchmarking

Abstract

We benchmark five MLP classifiers that differ only in the **output-layer** weight parameterization and noise injection: digital (baseline), multiplicative weight-noise ("amplitude"), multiplicative noise-aware training, cosine phase weights with phase noise, and phase noise-aware training. Across five datasets (MNIST, KMNIST, EMNIST Letters, CIFAR-10 flattened, Fashion-MNIST), we evaluate accuracy over fixed inference-noise grids and summarize per-dataset means and coarse robustness diagnostics (max–min over the grid). Under this setup (single training seed; single noise draw per σ), multiplicative noise-aware training nearly matches the digital baseline in mean accuracy (0.8329 vs 0.8359) while exhibiting reduced variation across the tested grids. Noise-aware training substantially improves the phase parameterization (mean $0.6156 \rightarrow 0.8002$), though phase remains weaker on CIFAR-10(flat) under the bounded $\cos(\theta)$ model. We provide configuration details and reproducibility commands, and outline controls and multi-draw/multi-seed extensions for stronger robustness claims.

1 Introduction

Analog neural accelerators promise energy and latency benefits but face device noise and variability. This work isolates the **output layer only** and compares analog-inspired weight encodings (amplitude, phase) against a digital MLP baseline across multiple datasets. We ask: (1) How close can these output-layer encodings get to digital accuracy? (2) How much does noise-aware training help? (3) How do results vary with dataset difficulty?

2 Models and Noise Modes

Scope clarification: only the output layer is "analog-modeled" (amplitude or phase perturbations); hidden layers remain digital. Non-idealities are injected per-weight, i.i.d., at inference (and optionally during training). Claims are limited to these output encodings, not full-stack analog accelerators (no ADC/DAC, drift, saturation, or multi-layer analog noise accumulation).

For input $x \in \mathbb{R}^d$ and class count C:

- **Digital**: standard MLP with hidden layers defined per dataset; logits are linear outputs over C classes.
- **Amplitude (multiplicative gain noise on signed weights)**: output weights W perturbed multiplicatively at inference:

$$W_{\text{noisy}} = W \odot (1 + \epsilon), \quad \epsilon \sim \mathcal{N}(0, \sigma_{\text{amp}}^2).$$

- **Amplitude_noiseaware**: same, but during training each forward pass samples σ_{amp} from a list (config `train_noise_list`).

- **Phase**: output weights encoded as $\cos(\Theta)$ with additive phase noise at inference:

$$\Theta \in \mathbb{R}^{d\times C}, \qquad \epsilon \sim \mathcal{N}(0, \sigma^2_{\text{phase}}) \text{ (elementwise)},$$
$$W = \cos(\Theta), \qquad W_{\text{noisy}} = \cos(\Theta + \epsilon), \qquad \text{logits} = x^\top W_{\text{noisy}} + b.$$

- **Phase_noiseaware**: same, but training samples σ_{phase} per forward pass from `train_noise_list`.

Loss is cross-entropy:

$$L = -\frac{1}{N}\sum_{i=1}^{N} \log\left(\text{softmax}(\text{logits}_i)_{y_i}\right).$$

Optimization uses Adam with dataset-specific learning rates and epochs from `config.yml`. Batch size is 128. Seeds: `numpy`/`torch` set to 42. Device selection prefers Metal (mps) → CUDA → CPU.

3 Datasets

- MNIST (10 classes, $28 \times 28 \to 784$).
- KMNIST (10 classes, $28 \times 28 \to 784$).
- EMNIST Letters (26 classes, $28 \times 28 \to 784$).
- CIFAR-10 (flattened, 10 classes, $32 \times 32 \times 3 \to 3072$).
- Fashion-MNIST (10 classes, $28 \times 28 \to 784$).

Architectures (`hidden_dims`) and training hyperparameters are defined per dataset in `config.yml`.

3.1 Key hyperparameters (from `config.yml`)

Dataset block	hidden_dims	epochs	lr	batch	input_dim	classes
digits_demo (MNIST)	[256, 128]	40	0.005	128	784	10
fashion_complex (FMNIST)	[512, 256, 128]	50	0.003	128	784	10
kmnist_benchmark	[512, 256]	45	0.0035	128	784	10
emnist_letters_benchmark	[512, 256, 128]	55	0.003	128	784	26
cifar10_flat_benchmark	[1024, 512, 256]	65	0.0025	128	3072	10

3.2 Noise grids (inference) and training noise lists

Noise is injected per-weight, i.i.d. at inference. For noise-aware variants, each forward pass samples σ uniformly from the training list.

Dataset block	noise_std (inference)	train_noise_list (phase/amplitude)
digits_demo	[0, 0.01, 0.02, 0.05, 0.1, 0.15, 0.2, 0.25, 0.3, 0.4]	[0.01, 0.02, 0.05, 0.08, 0.1, 0.15, 0.2]
fashion_complex	same as digits_demo	same as digits_demo
kmnist_benchmark	[0, 0.01, 0.02, 0.05, 0.1, 0.15, 0.2, 0.25, 0.3, 0.4]	[0.01, 0.02, 0.05, 0.08, 0.1, 0.15, 0.2]
emnist_letters_benchmark	[0, 0.01, 0.02, 0.05, 0.08, 0.12, 0.16, 0.2, 0.25, 0.3]	[0.01, 0.02, 0.05, 0.08, 0.12, 0.16, 0.2, 0.25]
cifar10_flat_benchmark	[0, 0.01, 0.02, 0.05, 0.08, 0.12, 0.16, 0.2, 0.25, 0.3]	[0.01, 0.02, 0.05, 0.08, 0.12, 0.16, 0.2, 0.25]

4 Experimental Setup

- **Training**: Adam; dataset-specific epochs, learning rates, hidden dimensions, class counts, batch size 128.
- **Noise sweeps**: inference noise standard deviations from each dataset's `noise_std` list; each σ applied to the corresponding mode (phase or amplitude) and accuracy recorded.
- **Noise-aware training**: if `train_noise_list` is provided, each forward pass samples σ uniformly and injects noise as above.
- **Single draw per σ**: for each σ, we draw one weight-perturbation tensor ϵ and evaluate accuracy over the full test set with that fixed perturbation.
- **Units**: for phase models, Θ and σ_{phase} are in radians; amplitude σ_{amp} is a dimensionless gain std.
- **Data splits**: training subset is 80% of the provided train set (chosen for runtime); evaluation on the official test set.
- **Transforms**: `ToTensor` + dataset-specific normalization + flatten.
- **Hardware**: auto-selected device (mps $\rightarrow$ cuda $\rightarrow$ cpu).
- **Determinism caveat**: single seed; MPS/CUDA may be non-deterministic; CPU can be used for stricter reproducibility (slower).

4.1 Reproduction Steps

1. MNIST: `python src/run_benchmark.py --config config.yml --csv results/mnist.csv --json results/mnist.json`
2. KMNIST: `python src/run_benchmark_fashion.py --config config.yml --config-key kmnist_benchmark --csv results/kmnist.csv --json results/kmnist.json`
3. EMNIST Letters: `python src/run_benchmark_fashion.py --config config.yml --config-key emnist_letters_benchmark --csv results/emnist.csv --json results/emnist.json`

4. CIFAR-10 (flat): `python src/run_benchmark_fashion.py --config config.yml --config-key cifar10_flat_benchmark --csv results/cifar10.csv --json results/cifar10.json`

5. Fashion-MNIST: `python src/run_benchmark_fashion.py --config config.yml --config-key fashion_complex --csv results/fmnist.csv --json results/fmnist.json`

6. Analysis & plots: `python scripts/analyze_benchmark.py`

5 Results

5.1 Aggregate (mean over five datasets; per-dataset means are over the evaluation noise grid; spread = max–min on single-draw curves)

Per-dataset mean accuracy is

$$a_k = \frac{1}{|\Sigma_k|} \sum_{\sigma \in \Sigma_k} \mathrm{Acc}(k, \sigma),$$

and the aggregate acc_mean averages a_k over the five datasets. For the digital baseline, we report standard test accuracy (equivalently $\Sigma_k = \{0\}$) and do not inject inference noise.

Model	acc_mean	acc_min	acc_max	diff (spread)
digital	0.8359	0.8359	0.8359	N/A (no noise)
amplitude	0.8302	0.8158	0.8343	0.0185
amplitude_noiseaware	0.8329	0.8310	0.8341	0.0031
phase	0.6156	0.2125	0.8406	0.6281
phase_noiseaware	0.8002	0.6964	0.8207	0.1243

Table 1: Aggregate accuracy and spread across five datasets. Per-dataset accuracies are averaged over the evaluation noise grid; spread is max–min on single-draw curves. Digital spread is undefined because no inference noise is applied. Amplitude denotes multiplicative gain noise on signed weights.

5.2 Per-dataset summaries (means, spreads; single seed, single noise draw per σ)

Dataset	digital	amplitude	amp_noiseaware	phase	phase_noiseaware
MNIST	0.9760	0.9730	0.9721	0.7842	0.9488
KMNIST	0.8913	0.8797	0.8878	0.7454	0.8530
EMNIST	0.9033	0.9009	0.8985	0.5690	0.8923
CIFAR10	0.5189	0.5149	0.5218	0.3119	0.4515
FMNIST	0.8899	0.8825	0.8844	0.6675	0.8553

Table 2: Per-dataset mean accuracies (averaged over the evaluation noise grid).

Dataset	digital	amplitude	amp_noiseaware	phase	phase_noiseaware
MNIST	0.0000	0.0081	0.0016	0.7033	0.1717
KMNIST	0.0000	0.0087	0.0055	0.5855	0.1781
EMNIST	0.0000	0.0339	0.0043	0.7881	0.0475
CIFAR10	0.0000	0.0250	0.0018	0.4011	0.0590
FMNIST	0.0000	0.0168	0.0024	0.6624	0.1652

Table 3: Per-dataset spreads (max–min over the evaluation noise grid; single draw per σ).

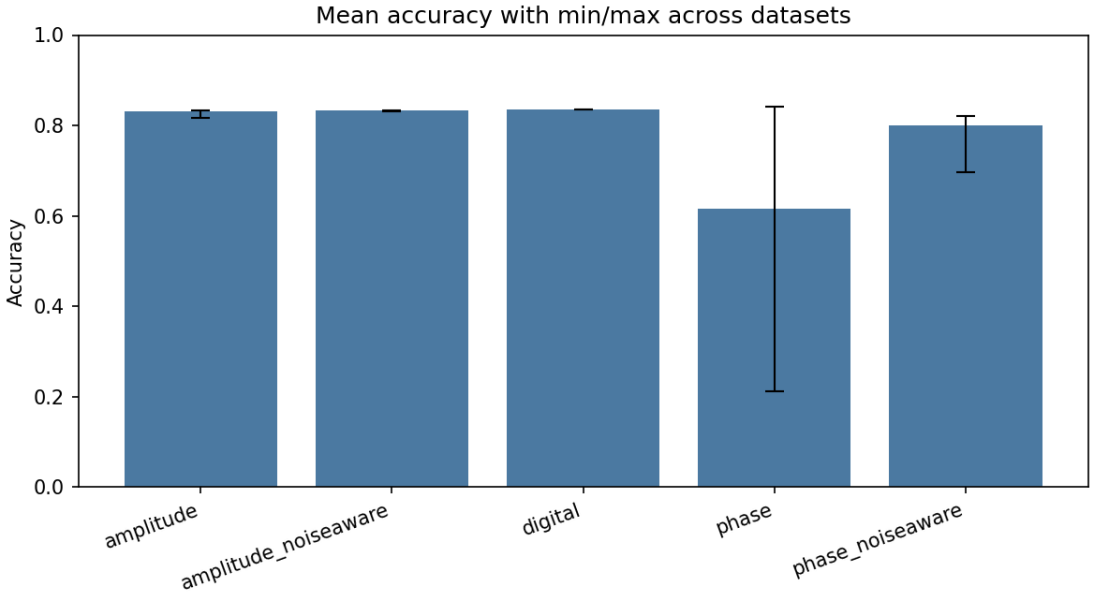

Figure 1: Mean accuracy with min/max error bars across datasets.

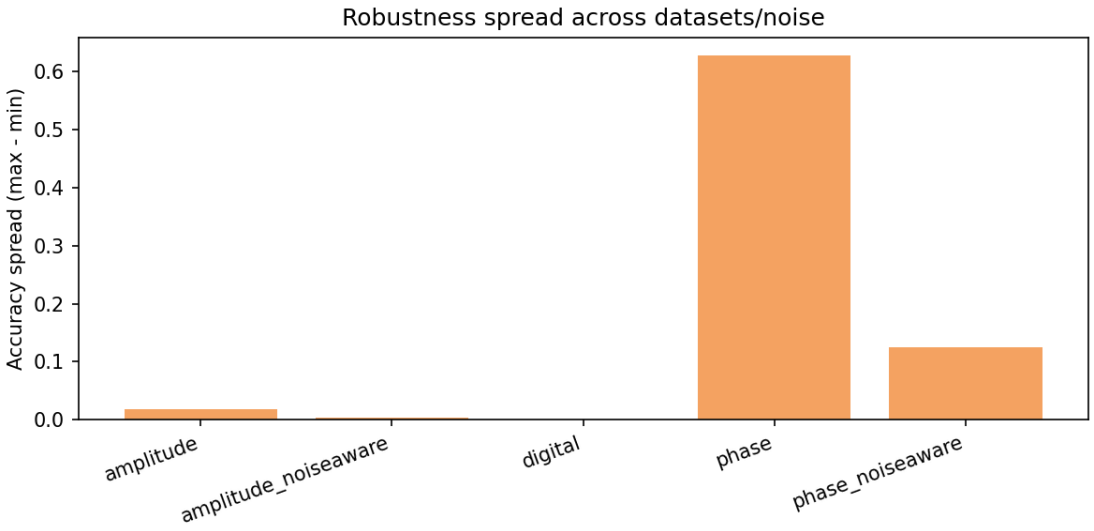

Figure 2: Accuracy spread (max–min) per model.

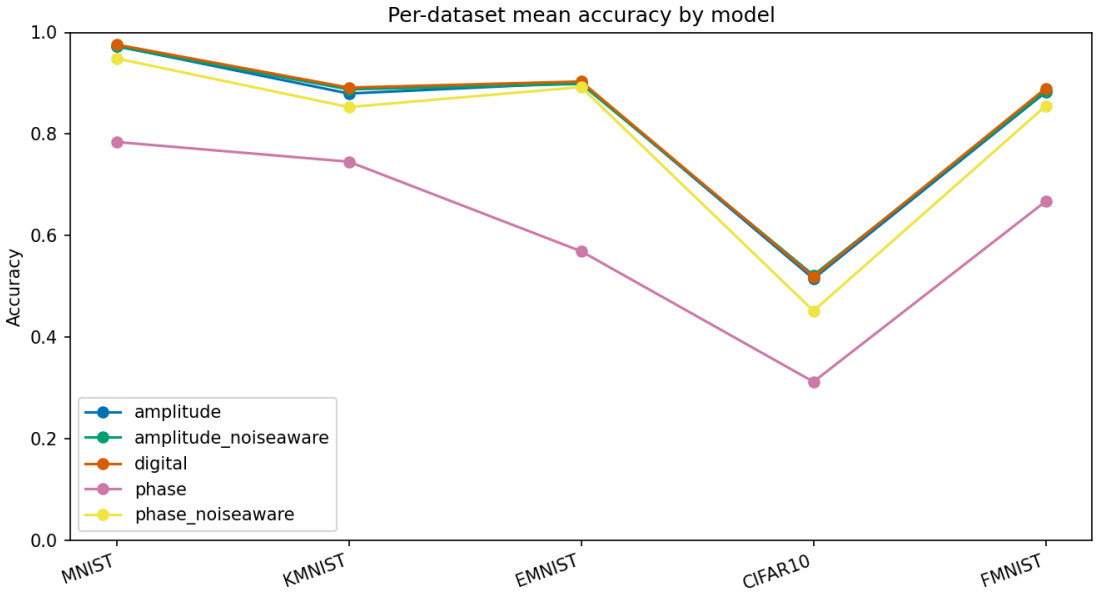

Figure 3: Per-dataset mean accuracy by model.

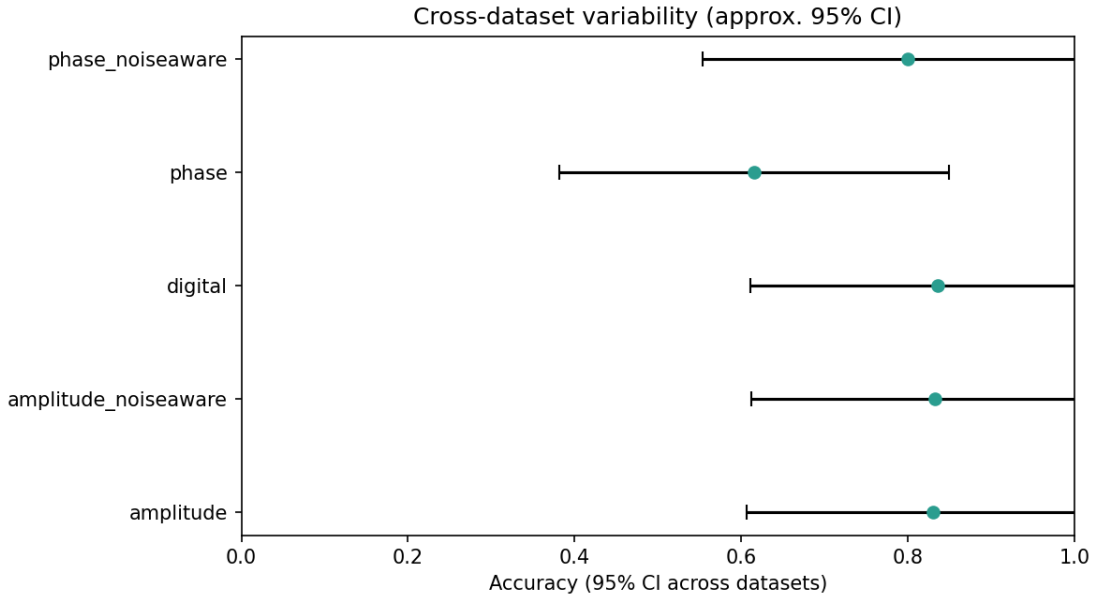

Figure 4: Cross-dataset variability interval (t-based, descriptive) for per-dataset mean accuracy.

5.3 Figures

6 Statistical Perspective

Let $n = 5$ datasets. We compute a t-based cross-dataset variability interval:

$$\bar{a} = \frac{1}{n}\sum_{k=1}^{n} a_k, \quad s = \sqrt{\frac{1}{n-1}\sum_{k=1}^{n}(a_k - \bar{a})^2}, \quad \text{VarInterval} = \bar{a} \pm t_{0.975,n-1}\frac{s}{\sqrt{n}}.$$

This reflects task difficulty variation, not a sampling CI. Because accuracies are bounded in $[0, 1]$, these intervals are descriptive dispersion summaries only. Summary (from `results/benchmark_stats_summary.cs`

- digital: 0.8359 ± 0.2244
- amplitude: 0.8302 ± 0.2238
- amplitude_noiseaware: 0.8329 ± 0.2205
- phase: 0.6156 ± 0.2343
- phase_noiseaware: 0.8002 ± 0.2467

Accuracy deltas vs digital (means): amplitude -0.0057; amplitude_noiseaware -0.0030; phase -0.2203; phase_noiseaware -0.0357. Robustness: amplitude_noiseaware spread is $\sim 6\times$ smaller than amplitude; phase_noiseaware spread is $\sim 5\times$ smaller than phase. Digital spread is undefined because no noise was injected into the baseline; a digital+noise control would allow direct robustness comparison.

7 Discussion

Noise-aware training consistently tightens spreads and boosts phase performance. The mean gap between amplitude_noiseaware and digital (≈ 0.003) is negligible relative to observed variation, making amplitude_noiseaware the *best-performing encoding under the tested assumptions*. Spread (max–min) is a coarse, outlier-sensitive diagnostic that depends on the chosen noise grid; we include it for quick comparison on a fixed grid rather than as a definitive robustness metric. Phase remains risky in this bounded $\cos(\theta)$ parameterization with unwrapped Gaussian noise; conclusions about phase are conditional on this capacity and noise model (unwrapped Gaussian used here for simplicity in the small-σ regime; wrapped models like von Mises are more appropriate for larger phase noise). Dataset difficulty matters: small grayscale digits are forgiving; CIFAR-10(flat) primarily tests representation capacity of flattened MLPs.

8 Implications for Output-Layer Encoding Choices

- Default to **amplitude_noiseaware** within this output-layer perturbation model for robustness with minimal accuracy loss.
- If using phase, always train noise-aware; plain phase is too unstable in this bounded $\cos(\theta)$ parameterization.
- For harder vision tasks, pair analog heads with stronger feature extractors (e.g., conv nets) before evaluating robustness.

9 Threats to Validity

Flattened CIFAR-10 should be read as a capacity/representation stress test for MLP heads rather than a canonical vision benchmark; convolutional features could alter rankings. Single-architecture MLP; deeper/wider networks may shift results. Formal significance testing across multiple seeds is not reported here; interpretations rely on effect sizes and spreads. Noise model may not capture all hardware non-idealities.

10 Controls and Future Improvements

- Add **digital + noise** controls (inference and noise-aware training) to separate encoding effects from regularization by noise.
- Increase robustness rigor: multiple seeds; multiple noise draws per σ; report worst-case accuracy and AUC over justified σ ranges.
- Phase capacity/noise model: consider $w = \alpha\cos(\theta)$ or I/Q ($a\cos\theta + b\sin\theta$); consider wrapped noise for larger σ.
- Use full train splits (or justify subsampling) and explore conv features for CIFAR-10.

11 Related Work (brief)

Phase/amplitude encodings in photonic and RF accelerators are sensitive to phase noise and amplitude drift; noise-aware or stochastic training has been proposed to improve robustness. Our findings align: injecting noise during training stabilizes inference under perturbations.

12 Conclusion

Under the tested assumptions (single seed; single noise draw per σ; fixed noise grids), amplitude_noiseaware offers the best observed balance of accuracy and robustness diagnostics across these datasets, approaching digital performance with minimal variation on the evaluated grids. Phase models require noise-aware training to be viable and still lag on challenging data in this bounded $\cos(\theta)$ parameterization. Future work should incorporate convolutional feature extractors, per-dataset noise curricula, formal significance tests versus digital baselines, and digital+noise controls.

Acknowledgments

We thank prior work on analog-inspired training and robustness; references omitted in this draft.

References (draft list)

Title	Year	Src.	Note
A Tutorial about Random Neural Networks in Supervised Learning (http://arxiv.org/abs/1609.04846v1)	2016	arXiv	Random neural networks / queueing view.
Predicting concentration levels of air pollutants by transfer learning and recurrent neural network (http://arxiv.org/abs/2502.01654v1)	2025	arXiv	Air pollution prediction.
Analog Alchemy: Neural Computation with In-Memory Inference, Learning and Routing (http://arxiv.org/abs/2412.20848v1)	2024	arXiv	In-memory analog neural computation and routing.
Masked Conditional Neural Networks for Audio Classification (http://arxiv.org/abs/1803.02421v2)	2018	arXiv	Conditional/masked neural networks for temporal signals.
The Deep Arbitrary Polynomial Chaos Neural Network (http://arxiv.org/abs/2306.14753v1)	2023	arXiv	Homogeneous chaos theory applied to deep networks.
A Neural Network-Evolutionary Computational Framework for RUL Estimation (http://arxiv.org/abs/1905.05918v1)	2019	arXiv	Remaining useful life estimation.
Memristors – from In-memory computing to Neuromorphic Computing (http://arxiv.org/abs/2004.14942v1)	2020	arXiv	Survey of memristor-based computing.
Reservoir Memory Machines as Neural Computers (http://arxiv.org/abs/2009.06342v2)	2020	arXiv	Differentiable neural computers with explicit memory.
Adversarial Frontier Stitching for Remote Neural Network Watermarking (http://arxiv.org/abs/1711.01894v2)	2017	arXiv	Watermarking neural networks via adversarial stitching.
A Review on Neural Network Models of Schizophrenia and ASD (http://arxiv.org/abs/1906.10015v2)	2019	arXiv	Survey of NN models of ASD and schizophrenia.
Structure Is Not Enough: Leveraging Behavior for Neural Network Weight Reconstruction (http://arxiv.org/abs/2503.17138v1)	2025	arXiv	Weight reconstruction using behavioral cues.
Adiabatic Fine-Tuning of Neural Quantum States (http://arxiv.org/abs/2503.17140v2)	2025	arXiv	Neural quantum states and phase transitions in weight space.
Encoding binary neural codes in networks of threshold-linear neurons (http://arxiv.org/abs/1212.0031v3)	2012	arXiv	Encoding patterns via synaptic connections.
Recursive Self-Similarity in Deep Weight Spaces of Neural Architectures (http://arxiv.org/abs/2503.14298v1)	2025	arXiv	Fractal/coarse geometry perspective on deep weight spaces.
Development of a sensory-neural network for medical diagnosing (http://arxiv.org/abs/1807.02477v1)	2018	arXiv	Sensory-neural network for diagnostics.
Normalisation of Weights and Firing Rates in Spiking Neural Networks with STDP (http://arxiv.org/abs/1910.00122v1)	2019	arXiv	Spiking homeostasis and normalization.
Implementing a Bayes Filter in a Neural Circuit (http://arxiv.org/abs/1512.07839v4)	2015	arXiv	Bayesian filtering with neural circuits.
On functions computed on trees (http://arxiv.org/abs/1904.02309v4)	2019	arXiv	Hierarchical function compositions on trees.
Coherent states for compact Lie groups and their large-N limits (http://arxiv.org/abs/1707.02355v1)	2017	arXiv	Survey of heat-kernel coherent states.

Title	Year	Src.	Note
Cognitive computation with autonomously active neural networks (http://arxiv.org/abs/0901.3028v1)	2009	arXiv	Self-sustained neural activity and cognition.
Coherent states in fermionic Fock-Krein spaces and their amplitudes (http://arxiv.org/abs/1708.03047v2)	2017	arXiv	Fermionic coherent states with indefinite inner products.
Review of Entangled Coherent States (http://arxiv.org/abs/1112.1778v1)	2011	arXiv	Survey of entangled coherent states.
Accumulate: An identity-based blockchain protocol (http://arxiv.org/abs/2204.06878v2)	2022	arXiv	DPoS blockchain with identity and cross-chain support.
Linear Delay-cell Design for Low-energy Delay Multiplication and Accumulation (http://arxiv.org/abs/2007.13895v3)	2020	arXiv	Low-energy MAC design.
MultiPLY: A Multisensory Object-Centric Embodied LLM in 3D World (http://arxiv.org/abs/2401.08577v1)	2024	arXiv	Multisensory object-centric embodied model.
AutoLungDx: A Hybrid Deep Learning Approach for Early Lung Cancer Diagnosis (http://arxiv.org/abs/2305.00046v4)	2023	arXiv	Hybrid 3D Res-U-Net/YOLOv5/ViT for lung cancer.
On the Capacity Region of the Two-User Interference Channel (http://arxiv.org/abs/1302.1837v1)	2013	arXiv	Interference channel capacity region.
A Multi-Stage Hybrid CNN-Transformer Network for Pediatric Lung Sound Classification (http://arxiv.org/abs/2507.20408v2)	2025	arXiv	Hybrid CNN-Transformer for lung sounds.
Interference Mitigation through Limited Transmitter Cooperation (http://arxiv.org/abs/1004.5421v1)	2010	arXiv	Cooperation strategies for interference mitigation.
A Self-Attention-Driven Deep Denoiser Model for Real Time Lung Sound Denoising (http://arxiv.org/abs/2404.04365v3)	2024	arXiv	Self-attention denoiser for lung sounds.
Call to Protect the Dark and Quiet Sky from Satellite Constellations (http://arxiv.org/abs/2412.08244v2)	2024	arXiv	Impact of satellite constellations on sky observations.
ResCap-DBP: Lightweight Residual-Capsule Network for DNA-Binding Protein Prediction (http://arxiv.org/abs/2507.20426v1)	2025	arXiv	Residual-capsule network for DBP prediction.
Piecewise Semi-Analytical Formulation for Coupled-Oscillator Systems (http://arxiv.org/abs/2404.12780v1)	2024	arXiv	Semi-analytical solutions for coupled oscillators.
How transferable are features in deep neural networks? (http://arxiv.org/abs/1411.1792v1)	2014	arXiv	Feature transferability in deep nets.
Parallel Neural Networks in Golang (http://arxiv.org/abs/2304.09590v1)	2023	arXiv	PNNs implemented in Go.
Dual Accuracy-Quality-Driven Neural Network for Prediction Interval Generation (http://arxiv.org/abs/2212.06370v4)	2022	arXiv	Uncertainty quantification with dual objectives.
Synchronization conditions in the Kuramoto model (http://arxiv.org/abs/2007.04343v2)	2020	arXiv	Synchronization conditions and seminorms.
Conformal Group Actions on Generalized Kuramoto Oscillators (http://arxiv.org/abs/1812.06539v3)	2018	arXiv	Group actions on generalized Kuramoto models.

Title	Year	Src.	Note
Synchronization of Kuramoto Oscillators on Knots (http://arxiv.org/abs/1104.3493v2)	2011	arXiv	Knot-based oscillator synchronization.
Compute and Energy Consumption Trends in Deep Learning Inference (http://arxiv.org/abs/2109.05472v2)	2021	arXiv	Trends in compute and energy for DL inference.
Cold Start Latency in Serverless Computing (http://arxiv.org/abs/2310.08437v2)	2023	arXiv	Review of cold start latency in serverless.
Solving the Hamiltonian path problem with a light-based computer (http://arxiv.org/abs/0708.1512v1)	2007	arXiv	Optical approach to Hamiltonian path.
Quantum Computing: Vision and Challenges (http://arxiv.org/abs/2403.02240v5)	2024	arXiv	Vision and challenges in quantum computing.
Tierkreis: A Dataflow Framework for Hybrid Quantum-Classical Computing (http://arxiv.org/abs/2211.02350v1)	2022	arXiv	Dataflow framework for hybrid quantum-classical.
Synthetic Biology meets Neuromorphic Computing (http://arxiv.org/abs/2504.10053v2)	2025	arXiv	Bio-inspired olfactory perception system.
Double Robust Semi-Supervised Inference for the Mean (http://arxiv.org/abs/2104.06667v2)	2021	arXiv	Semi-supervised inference under MAR labeling.
A Comparative Study of Load Balancing Algorithms in Cloud Computing Environment (http://arxiv.org/abs/1403.6918v1)	2014	arXiv	Load balancing in cloud environments.
Universal Workers: A Vision for Eliminating Cold Starts in Serverless Computing (http://arxiv.org/abs/2505.19880v2)	2025	arXiv	Reducing cold starts in serverless computing.
Placement of Microservices-based IoT Applications in Fog Computing (http://arxiv.org/abs/2207.05399v2)	2022	arXiv	Taxonomy for fog computing placement.
Driven spin wave modes in XY ferromagnet (http://arxiv.org/abs/1706.01619v6)	2017	arXiv	Nonequilibrium phase transition in XY ferromagnets.
Room temperature reversible colossal volto-magnetic effect (http://arxiv.org/abs/2308.04324v1)	2023	arXiv	Volto-magnetic effect in oxide heterostructures.
Reversible Computing with Fast, Fully Static, Fully Adiabatic CMOS (http://arxiv.org/abs/2009.00448v2)	2020	arXiv	Energy-efficient reversible CMOS.
Monte Carlo study of the phase transitions in the classical XY ferromagnets (http://arxiv.org/abs/2208.10109v8)	2022	arXiv	Monte Carlo of anisotropic XY ferromagnets.
Supporting Multi-Cloud in Serverless Computing (http://arxiv.org/abs/2209.09367v4)	2022	arXiv	Multi-cloud strategies for serverless.
Bridging Phases at the Morphotropic Boundaries of Lead-Oxide Solid Solutions (http://arxiv.org/abs/cond-mat/0511256v1)	2005	arXiv	Piezoelectric solid solutions near morphotropic boundaries.
Graph Neural Networks Based Analog Circuit Link Prediction (http://arxiv.org/abs/2504.10240v5)	2025	arXiv	GNNs for analog circuit link prediction.
Partially Oblivious Neural Network Inference (http://arxiv.org/abs/2210.15189v1)	2022	arXiv	Oblivious inference for privacy.
A Metalearned Neural Circuit for Nonparametric Bayesian Inference (http://arxiv.org/abs/2311.14601v1)	2023	arXiv	Meta-learned neural circuit for Bayesian inference.
On the Accuracy of Analog Neural Network Inference Accelerators (http://arxiv.org/abs/2109.01262v3)	2021	arXiv	Accuracy analysis of analog NN accelerators.

Title	Year	Src.	Note
DiffCkt: A Diffusion Model-Based Hybrid Neural Network Framework for Automatic Transistor-Level Generation of Analog Circuits (http://arxiv.org/abs/2507.00444v2)	2025	arXiv	Diffusion + hybrid NN for analog circuit generation.
The CEPC input for the European Strategy for Particle Physics - Accelerator (http://arxiv.org/abs/1901.03169v1)	2019	arXiv	CEPC accelerator design summary.
Applications of Particle Accelerators (http://arxiv.org/abs/2407.10216v1)	2024	arXiv	Overview of particle accelerator applications.
Accelerator design concept for future neutrino facilities (http://arxiv.org/abs/0802.4023v2)	2008	arXiv	Scoping study findings for future neutrino facilities.
Time-domain and Frequency-domain Signals and their Analysis (http://arxiv.org/abs/2009.14544v2)	2020	arXiv	Signals in time/frequency domains.
Fixed-Field Alternating-Gradient Accelerators (http://arxiv.org/abs/1604.05221v1)	2016	arXiv	Overview of FFAG accelerators for medical applications.
Training of mixed-signal optical convolutional neural network with reduced quantization level (http://arxiv.org/abs/2008.09206v1)	2020	arXiv	Mixed-signal optical CNN training.
Analog, In-memory Compute Architectures for Artificial Intelligence (http://arxiv.org/abs/2302.06417v1)	2023	arXiv	Energy-efficiency limits in analog in-memory computing.
HZO-based FerroNEMS MAC for In-Memory Computing (http://arxiv.org/abs/2208.06499v1)	2022	arXiv	Ferroelectric NEMS unimorph for low-energy MAC.
MRAM-based Analog Sigmoid Function for In-memory Computing (http://arxiv.org/abs/2204.09918v1)	2022	arXiv	Analog sigmoid using MRAM.
An Asynchronous Multi-Beam MAC Protocol for Multi-Hop Wireless Networks (http://arxiv.org/abs/2111.10073v1)	2021	arXiv	Multi-beam MAC for wireless networks.
Wireless sensors networks MAC protocols analysis (http://arxiv.org/abs/1004.4600v1)	2010	arXiv	MAC protocols for wireless sensor networks.
Energy Efficient Dual Designs of FeFET-Based Analog In-Memory Computing (http://arxiv.org/abs/2410.19593v1)	2024	arXiv	FeFET-based IMC with shift-add capability.
LionHeart: A Layer-based Mapping Framework for Heterogeneous Systems with Analog In-Memory Computing Tiles (http://arxiv.org/abs/2401.09420v3)	2024	arXiv	Mapping framework for analog IMC tiles.
Nonlinear Integrated Microwave Photonics (http://arxiv.org/abs/1310.4897v1)	2013	arXiv	Nonlinear optical effects on chip.
Crosstalk Reduction for Superconducting Microwave Resonator Arrays (http://arxiv.org/abs/1206.5571v1)	2012	arXiv	Crosstalk reduction in MKIDs.
Near-Field Microwave Microscopy of Materials Properties (http://arxiv.org/abs/cond-mat/0001075v2)	2000	arXiv	Near-field microwave microscopy.
Bell-state measurement and quantum teleportation using linear optics (http://arxiv.org/abs/1304.1214v1)	2013	arXiv	Bell-state measurement and teleportation schemes.

Title	Year	Src.	Note
Enabling Scalable Photonic Tensor Cores with Polarization-Domain Photonic Computing (h t tp : //arxiv.org/abs/2501.18886v1)	2025	arXiv	Polarization-domain photonic tensor core.
Highly-coherent stimulated phonon oscillations in a multi-core optical fiber (http://arxiv.org/abs/1811.06290v1)	2018	arXiv	Coherent acoustic waves in multi-core fiber.
The COHERENT Experiment at the Spallation Neutron Source (http://arxiv.org/abs/1509.08702v2)	2015	arXiv	COHERENT CEvNS experiment overview.
CORE – a COmpact detectoR for the EIC (http://arxiv.org/abs/2209.00496v1)	2022	arXiv	CORE detector proposal for EIC.
COHERENT Collaboration data release from the first detection of CEvNS on argon (http://arxiv.org/abs/2006.12659v2)	2020	arXiv	COHERENT argon CEvNS data release.
An optical fiber-based probe for photonic crystal microcavities (http://arxiv.org/abs/physics/0406129v1)	2004	arXiv	Fiber probe for photonic crystal cavities.
Photovoltaic-ferroelectric materials for the realization of all-optical devices (http://arxiv.org/abs/2203.06515v1)	2022	arXiv	Photovoltaic-ferroelectric materials for optical devices.
Frequency Ratio Measurements with 18-digit Accuracy Using a Network of Optical Clocks (http://arxiv.org/abs/2005.14694v1)	2020	arXiv	Optical clock frequency ratio measurements.
A Fast, robust algorithm for power line interference cancellation in neural recording (http://arxiv.org/abs/1402.6862v2)	2014	arXiv	Power line interference cancellation.
Understanding and mitigating noise in trained deep neural networks (http://arxiv.org/abs/2103.07413v3)	2021	arXiv	Noise in trained DNNs and mitigation.
Denoising Noisy Neural Networks: A Bayesian Approach with Compensation (http://arxiv.org/abs/2105.10699v3)	2021	arXiv	Bayesian denoising for noisy neural networks.
Noise and Bell's inequality (http://arxiv.org/abs/1008.0667v2)	2010	arXiv	Noise considerations in Bell tests.
Quantum and Classical Frontiers of Noise (http://arxiv.org/abs/1612.03430v1)	2016	arXiv	Survey of quantum/classical noise frontiers.
Noise based logic: why noise? (http://arxiv.org/abs/1204.2545v4)	2012	arXiv	Noise-based logic and randomness.
Decoherence and noise in open quantum system dynamics (http://arxiv.org/abs/1605.07838v1)	2016	arXiv	Decoherence and noise in open systems.
Instantaneous noise-based logic (http://arxiv.org/abs/1004.2652v2)	2010	arXiv	Deterministic logic with binary noise timefunctions.
Noise Dynamics in the Quantum Regime (http://arxiv.org/abs/2311.17794v1)	2023	arXiv	Time-dependent modulation of current fluctuations.
Simple Cracking of (Noise-Based) Dynamic Watermarking in Smart Grids (http://arxiv.org/abs/2406.15494v3)	2024	arXiv	Security analysis of noise-based watermarking.
Phase-Locked, Low-Noise, Frequency Agile Titanium: Sapphire Lasers (http://arxiv.org/abs/physics/0507187v2)	2005	arXiv	Phase-locked Ti:sapphire lasers with low noise.

Title	Year	Src.	Note
Stokes' Drift and Hypersensitive Response with Dichotomous Markov Noise (http://arxiv.org/abs/cond-mat/0501499v1)	2005	arXiv	Stochastic Stokes' drift under dichotomous noise.
Shot noise for entangled and spin-polarized electrons (http://arxiv.org/abs/cond-mat/0210498v1)	2002	arXiv	Shot noise in entangled/spin-polarized transport.
The Data Conversion Bottleneck in Analog Computing Accelerators (http://arxiv.org/abs/2308.01719v4)	2023	arXiv	Data conversion limits in analog accelerators.
Analysis of Performance of Linear Analog Codes (http://arxiv.org/abs/1511.05509v2)	2015	arXiv	MSE performance bounds for linear analog codes.
Security of quantum key distribution with detection-efficiency mismatch (http://arxiv.org/abs/1810.04663v3)	2018	arXiv	Bounds for QKD with detector mismatch.
Performance Analysis of the Matrix Pair Beamformer with Matrix Mismatch (http://arxiv.org/abs/1009.5979v4)	2010	arXiv	Robustness of matrix pair beamformer.
The three and a half layers of dynamics : analog, digital, semi-digital, analog (http://arxiv.org/abs/1106.0911v1)	2011	arXiv	Perspective on analog/digital dynamics.
Are Bohmian trajectories real? (http://arxiv.org/abs/quant-ph/0609172v2)	2006	arXiv	Bohmian trajectories and classical mismatch.
Computation over Mismatched Channels (http://arxiv.org/abs/1204.5059v2)	2012	arXiv	Distributed computation over MAC with mismatch.
Superfluid Analog of the Davies-Unruh Effect (http://arxiv.org/abs/gr-qc/0505005v1)	2005	arXiv	Analog of Davies-Unruh in superfluid helium.
Semantic Communications with Discrete-time Analog Transmission: A PAPR Perspective (http://arxiv.org/abs/2208.08342v3)	2022	arXiv	Semantic communications with analog transmission.
Programmable photonic circuits (https://doi.org/10.1038/s41566-020-0585-z)	2020	bib	Overview of programmable photonic circuits.
Coupled oscillators for computing: A review and perspective (https://doi.org/10.1063/1.5108897)	2020	bib	Review of coupled oscillator computing.
Parallel convolutional processing using an integrated photonic tensor core (https://doi.org/10.1038/s41586-020-03070-1)	2021	bib	Photonic tensor core for convolutions.
Oscillatory neurocomputers with dynamic connectivity (https://doi.org/10.1126/science.283.5408.1903)	1999	bib	Oscillatory neurocomputer concept.
A 65nm 4.7TOPS/W 8bit CNN processor with mixed-signal computing (https://doi.org/10.1109/ISSCC.2018.8310344)	2018	bib	Mixed-signal CNN accelerator with calibration.
All-optical machine learning using diffractive deep neural networks (https://doi.org/10.1126/science.aat8084)	2018	bib	Diffractive optical layers performing inference.
Noise mitigation in analog in-memory computing for deep neural network accelerators (https://doi.org/10.1109/JXCDC.2021.3090030)	2021	bib	Noise mitigation for analog IMC accelerators.

Title	Year	Src.	Note
Experimental demonstration of reservoir computing on a silicon photonics chip (https://doi.org/10.1038/ncomms3541)	2014	bib	Photonic reservoir computing demonstration.
Broadcast and weight: An integrated network for scalable photonic spike processing (https://doi.org/10.1038/srep05522)	2014	bib	Photonic weighting for neuromorphic spikes.
Optimal design for universal multiport interferometers (https://doi.org/10.1364/OPTICA.3.001460)	2016	bib	Mesh design for programmable interferometers.
Memory devices and applications for in-memory computing (https://doi.org/10.1038/s41565-020-0655-z)	2020	bib	Survey of memory devices for IMC.
Deep learning with coherent nanophotonic circuits (https://doi.org/10.1038/nphoton.2017.93)	2017	bib	Phase-programmable nanophotonic interferometer.
Neuromorphic photonic networks using silicon photonic weight banks (https://doi.org/10.1038/s41598-017-06630-y)	2017	bib	Photonic weight banks for coherent summation.
An oscillator-based Ising machine (https://doi.org/10.1038/s41928-019-0300-0)	2019	bib	Oscillator-based Ising machine.
Deep physical neural networks trained with backpropagation (https://doi.org/10.1038/s41586-021-04223-6)	2022	bib	Backpropagation through physical systems.

A Full Tables

A.1 MNIST

model	acc_mean	acc_min	acc_max	diff
digital	0.976	0.976	0.976	0
amplitude	0.97297	0.9668	0.9749	0.0081
amplitude_noiseaware	0.97214	0.971	0.9726	0.0016
phase	0.78415	0.2754	0.9787	0.7033
phase_noiseaware	0.94876	0.802	0.9737	0.1717

A.2 KMNIST

model	acc_mean	acc_min	acc_max	diff
digital	0.8913	0.8913	0.8913	0
amplitude	0.87966	0.8733	0.882	0.0087
amplitude_noiseaware	0.88777	0.8846	0.8901	0.0055
phase	0.7454	0.3103	0.8958	0.5855
phase_noiseaware	0.85296	0.7051	0.8832	0.1781

A.3 EMNIST Letters

model	acc_mean	acc_min	acc_max	diff
digital	0.903317	0.903317	0.903317	0
amplitude	0.900913	0.873413	0.907260	0.033846
amplitude_noiseaware	0.898534	0.895625	0.899904	0.004279
phase	0.568952	0.122837	0.910913	0.788077
phase_noiseaware	0.892322	0.855	0.9025	0.0475

A.4 CIFAR-10 (flattened)

model	acc_mean	acc_min	acc_max	diff
digital	0.5189	0.5189	0.5189	0
amplitude	0.51489	0.4967	0.5217	0.025
amplitude_noiseaware	0.52177	0.5208	0.5226	0.0018
phase	0.31185	0.1246	0.5257	0.4011
phase_noiseaware	0.45151	0.4057	0.4647	0.059

A.5 Fashion-MNIST

model	acc_mean	acc_min	acc_max	diff
digital	0.8899	0.8899	0.8899	0
amplitude	0.88249	0.8687	0.8855	0.0168
amplitude_noiseaware	0.88441	0.8829	0.8853	0.0024
phase	0.66751	0.2295	0.8919	0.6624
phase_noiseaware	0.8553	0.714	0.8792	0.1652